LHCb-PUB-2009-013
August 26, 2009

The Muon Identification Procedure of the LHCb Experiment for the First Data

G. Lanfranchi[1], X. Cid Vidal[2], S. Furcas[1], M. Gandelman[3], J. A. Hernando[4], J. H. Lopez[3], E. Polycarpo[3], A. Sarti[1]

[1] *INFN - Laboratori Nazionali di Frascati, Italy*
[2] *Universidade de Santiago de Compostela, Spain*
[3] *Instituto de Fisica - Universidade Federal do Rio de Janeiro (UFRJ), Brazil*
[4] *CERN, Switzerland*[1]

Abstract

We present a refined muon identification algorithm for the LHCb experiment suitable for the first period of data taking. The new algorithm is robust against possible inefficiencies of the Muon Detector and takes properly into account the momentum dependence, so it can be tuned with calibration samples and exported to signal samples with different momentum spectra without large corrections.

The average performance depends on the momentum spectrum of the analyzed sample: with the current simulation we find for tracks with $p > 3$ GeV/c in a generic b-inclusive sample a muon identification efficiency of 90% for a misidentification rate of hadrons and electrons of $\sim$2.4% ($\sim$ 1% excluding π's and K's decays in flight).

Additional rejection power can be obtained by combining in a proper way the informations coming from all the other subdetectors in a global Likelihood: in this case for a muon identification efficiency of 90% we find a misidentification rate of $\sim$1.8% ($\sim$ 0.8% excluding π's and K's decays in flight).

[1] On leave from Universidade de Santiago de Compostela, Spain

Contents

1 Introduction

The LHCb experiment is expected to collect its first data in the 2009-2010 run.

In this note we present a refined algorithm for the muon identification (MuonID) in LHCb suited for the first period of data taking: this procedure is robust to cope with a detector still not working in optimal conditions and easy to be calibrated with control channels.

The present note must be considered together with the note describing the calibration strategy [1] in order to understand the overall procedure: in fact the algorithm itself has been developed also taking into account its calibration with control samples and that this calibration has to be quick enough to allow data to be reconstructed quasi real time. In a second phase of the experiment, when the detector performance will be understood, more sophisticated methods can be used [2].

The MuonID algorithm used so far in the LHCb Monte Carlo simulation [3] has some limitations as far as its applicability to real data is concerned: the algorithm efficiency is strongly dependent on small variations of muon detector performance and its fine-tuning is very much dependent on the specific sample used to calibrate it. As a consequence, if applied to real data, it would require continuous monitoring of the muon detector performance and a complicated way to export the results obtained with a calibration sample to any other sample of interest.

In order to improve the performance stability against the variations of detector conditions and to make it easier to calibrate through control samples, several solutions are under study. Here we present in details one possible solution and its applicability to real data. The note is structured as follows: in Section 2 we review the Muon detector structure, in Section 3 we list the Monte Carlo samples used in this study, in Section 4 we summarize the main steps of the MuonID procedure used so far in the Monte Carlo simulation, in Section 5 we point out the main limitations of the current algorithm and we describe the new procedure, in Section 6 we show the results obtained with the current Monte Carlo simulation. Finally in Section 7 we show how we can reduce the misidentification rate by using in a simple way the calorimeters informations.

2 The Muon Detector

The muon system for the LHCb experiment [4] consists of five tracking stations placed along the beam axis and separated by iron filters.

The first station (M1) is placed in front of the calorimeter pre shower, at 12.1 m from the interaction point, and is important for the transverse-momentum measurement of the muon track used in the Level-0 muon trigger.

The remaining four stations are interleaved with the muon shield at mean positions of 15.2 m (M2), 16.4 m (M3), 17.6 m (M4) and 18.8 m (M5). The shield consists of the electromagnetic and hadronic calorimeters (in front of M2) and three 80 cm thick iron

	M1	M2	M3	M4	M5
R1	10×25	6.3×31.3	6.7×33.7	29×36	31×39
R2	20×25	12.5×62.5	13.5×67.5	58×72	62×77
R3	40×100	25×125	27×135	116×145	124×155
R4	80×200	50×250	54×270	131×290	248×309

Table 1: The logical pad size (in mm^2) in the four regions of each station.

filters for a total absorber-thickness of 20 nuclear interaction-lengths. The inner and outer angular acceptances of the muon system are 20 (16) mrad and 306 (258) mrad in the bending (non-bending) plane, similar to that of the tracking system. This provides a geometrical acceptance of about $\sim 20\,\%$ for muons from b decays relative to the full solid angle.

Each station is subdivided in four regions with dimensions and logical pad size which scales a factor two from one region to the next (Figure 1).

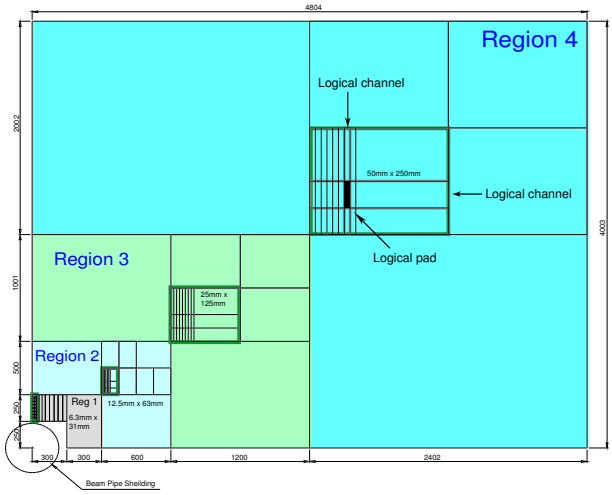

Figure 1: Front view of one quadrant of muon station 2, showing the dimensions of the regions. Inside each region is shown a sector defined by the size of the horizontal and vertical strips. The intersection of the horizontal and vertical strips, corresponding to the logical channels, are defined as logical pads. The region and channel dimensions scale by a factor two from one region to the next.

Since the absorber seen by a particle coming from the interaction point increases with the distance from the beam axis, and so the multiple scattering which limits the spatial resolution, the granularity of the detector varies accordingly. The logical pad dimension has been chosen such that its contribution to the p_T resolution is approximately equal to the multiple-scattering contribution. In Table 1 we show the logical pad sizes in the four regions of each station.

The muon stations are equipped with Multi Wire Proportional Chambers [4] (MW-

PCs) operating with an Ar:CO_2:CF_4 (40%:55%:5 % in volume) gas mixture. A detailed description and the results obtained from test beams is reported in [5, 6, 7]. At the nominal working point the measured MWPC efficiency is ϵ(MWPC)$\sim$ 99.5%.

3 Monte Carlo samples

The Monte Carlo samples used in this note are listed in Table 2.

channels	number of events	Configuration
b-inclusive	$\sim$ 100k	DC06-stripping-v31-lumi2
$J/\Psi \to \mu\mu$ inclusive	$\sim$ 100k	DC06-stripping-v31-lumi2
Minimum Bias	$\sim 4.2 \times 10^6$	DC06-L0-v1-lumi2

Table 2: Monte Carlo samples. The last column gives the configuration used in the LHCb bookkeeping database.

All the samples belong to the same Monte Carlo production set and have been produced assuming an average luminosity of $L = 2 \times 10^{32}$ cm^{-2} s^{-1}. In all the samples muons and hadrons decaying and non-decaying in flight are identified by using the Monte Carlo truth. The tracks in all the samples have been preselected by requiring to be long or downstream tracks[2] with a minimum momentum of $p = 3$ GeV/c and pointing inside the muon detector acceptance.

The b-inclusive sample is taken as a reference sample to extract the performance and compare results with the old algorithm. The $J/\Psi \to \mu\mu$ inclusive decay and the $\Lambda(1115.7) \to \pi p$ modes are the calibration samples that will be used in real data to tune the parameters of the algorithm and extract its performance, as described in [1]. In the present note the calibration samples are used to parameterize the curves that define the DLL. The $\Lambda(1115.7) \to p\pi$ sample is extracted from a minimum bias sample, as in LHCb no dedicated Monte Carlo production has been foreseen. For $J/\Psi \to \mu\mu$ and $\Lambda(1116) \to \pi p$ we consider only events selected as described in [1].

4 The MuonID procedure for an ideal detector

The MuonID algorithm used so far in Monte Carlo simulations [3] consists of two main steps:

1. **IsMuon definition:** given a reconstructed track in the LHCb tracking system, hits in the Muon stations are searched around the track extrapolation in some Field of Interest (*FOI*). A boolean decision (*IsMuon*) is applied to tracks which satisfy the

[2] A track is *long* if it comes from the primary vertex and releases hits in all the tracking detectors, it is *downstream* if releases hits only in the TT and IT/OT detectors [8].

requirement to have at least one hit in FOI in a number of stations which depends on the momentum of the track. The stations required by the IsMuon decision are shown in Table 3 as a function of the track momentum.

momentum range	muon stations
3 GeV/c $< p <$ 6 GeV/c	M2+M3
6 GeV/c $< p <$ 10 GeV/c	M2+M3+(M4.or.M5)
$p >$ 10 GeV/c	M2+M3+M4+M5)

Table 3: Muon stations required to trigger the IsMuon decision as a function of momentum range.

2. **The Delta Log Likelihood definition:** with the tracks surviving the IsMuon requirement, a Delta Log Likelihood (DLL) function is built defined as:

$$DLL = log(P_{\mu}/P_{\mathrm{non}-\mu}) \tag{1}$$

where P_{μ} and $P_{\mathrm{non}-\mu}$ are observables related to the probability for a given track to be compatible with the muon and non-muon hypothesis. The current algorithm uses as estimator of these two quantities the height of the normalized distributions for muons and non-muons of the average squared distance D of hits with respect to track extrapolation:

$$D = \sum_{i=0}^{N} \frac{1}{N} \left\{ \left(\frac{x_i - x_{track}}{pad_x} \right)^2 + \left(\frac{y_i - y_{track}}{pad_y} \right)^2 \right\} \tag{2}$$

where the sum runs over all the hits in the field of interest. The distance of the muon hits to the track extrapolation in a given station and region is normalized to the readout granularity of the muon detector in that station/region (Table 1).

The normalized distributions for muons and non-muons used to evaluate the DLL in [3] are extracted from a b-inclusive sample and fitted with a double Landau function, as shown in Figure 2.

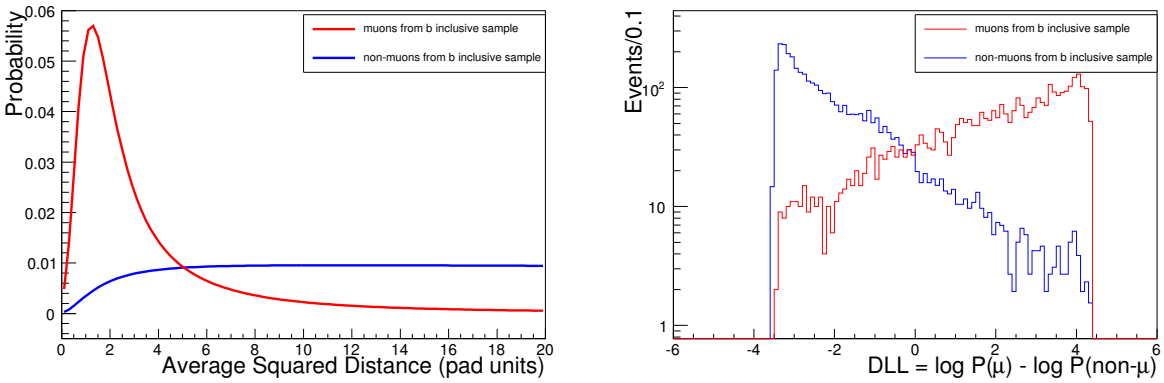

Figure 2: Average squared distance for muons and non-muons (left) and DLL (right) as defined in the text.

5 The MuonID procedure for a real detector

The main limitations of the procedure used so far in Monte Carlo simulation [3] are the following:

1. the IsMuon decision is a boolean decision: yes/no answer depends on number of hits in momentum bins (Table 3). In reality the probability to have a muon hit in a given station is a smooth function of the momentum p as shown in Figure 3. These curves define the probability that a muon with a given momentum p releases a hit in FOI in a given Muon Station.

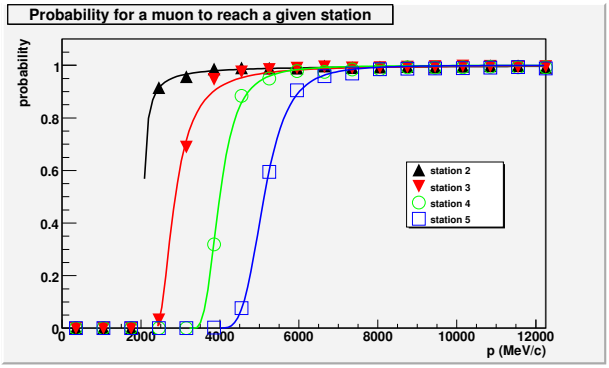

Figure 3: Probability for muon tracks to reach a given station as a function of momentum. These curves are obtained with true muons from a J/$\psi \to \mu\mu$ inclusive sample.

2. The IsMuon decision requires at least one hit in all the stations listed in Table 3. This requirement determines a strong dependence of the algorithm efficiency on variations in time and space of the muon chambers efficiencies as it asks for the AND of all the concerned stations. In fact, if k is the average efficiency loss in the MWPCs, the total efficiency loss in the muon identification procedure for any di-muon channel in the limit where k is small, will be:

$$\epsilon(2\mu) = (1-k)^n \simeq 1 - n \times k$$

where n is the number of stations involved to identify the two muons. For tracks with $p > 10$ GeV/c, $n = 2 \times 4 = 8$, which means that for every 1% efficiency loss in the chambers we loose as much as $\sim 8\%$ of di-μ events.

In Figure 4 (left) we show the impact on the MuonID efficiency for one muon from a prompt $J/\Psi \to \mu^+\mu^-$ sample due to an average loss of $2, 4, 6, 8\%$ in the MWPC efficiency with respect to its nominal value ($\epsilon \sim 99.5\%$). In the same Figure (right) we show the effect of an average loss of MWPC chambers efficiency of $\sim 3\%$ in the reconstruction of the two muons from $J/\Psi \to \mu\mu$ events. We see that the overall efficiency loss is $\sim 20\%$.

An average loss of $\sim 3\%$ over the whole detector must be considered an extreme case. However, mainly at the beginning of data taking, local inefficiencies might not be

unlikely as a result of a still non-optimal working point. Moreover local inefficiencies can affect in a different way different samples, since the detector illumination varies accordingly to the p and p_t spectrum of the involved tracks.

For example, in Figure 5 we show the impact on the MuonID efficiency for two muons from a prompt $J/\Psi \rightarrow \mu^+\mu^-$ sample due to an average loss of 3% in the MWPC efficiency with respect to its nominal value in regions R1-R2 only (upper left plot) and in regions R3-R4 only (upper right plot). The effect on the MuonID efficiency curve is different as different regions cover different momentum ranges: high momentum particles are more concentrated towards inner regions (Figure 5, bottom left), while low momentum particles are mostly in the outer regions (Figure 5, bottom right).

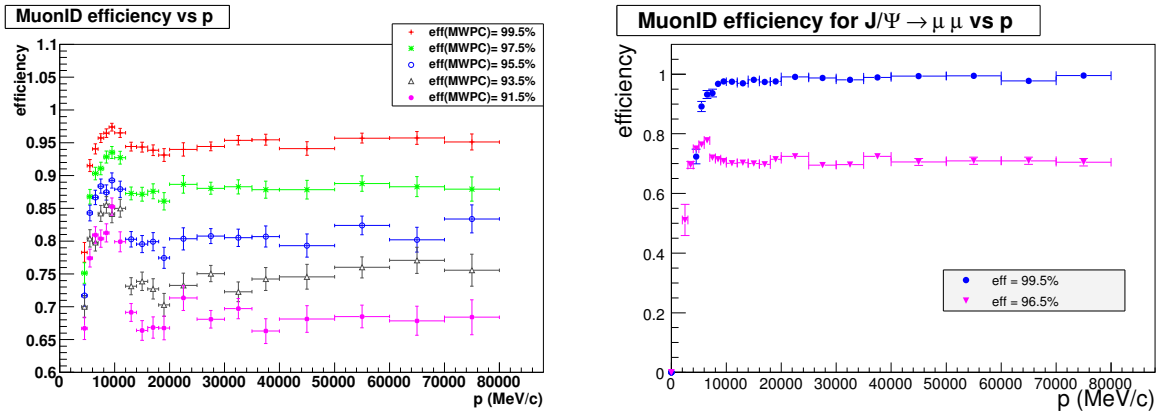

Figure 4: Muon identification efficiency for muons coming from a prompt J/Ψ decay as a function of the muon momentum. Left: efficiency of IsMuon requirement on a single muon as a function of momentum and MWPC efficiency. Right: efficiency of IsMuon requirement on two muons as a function of momentum for MWPCs working in nominal conditions ($\langle\epsilon\rangle = 99.5\%$) (blue dots) and working with $\langle\epsilon\rangle \sim 96.5\%$ (purple triangles). The values of MWPC efficiency are average values over all the detector stations.

3. The average squared distance distributions (Figure 2) are momentum dependent as they depend on the multiple scattering. For example Figure 6 shows the distribution of the D variable for muons from prompt $J/\Psi \rightarrow \mu^+\mu^-$ decay in two different momentum ranges, 3 GeV/c $< p <$ 10 GeV/c and $p >$ 30 GeV/c. Therefore a single curve obtained with a specific sample needs a proper momentum re weighting when being exported to other samples with different momentum spectrum.

The procedure described in the next Sections takes properly into account the momentum dependence and is more robust against possible variations of detector performance.

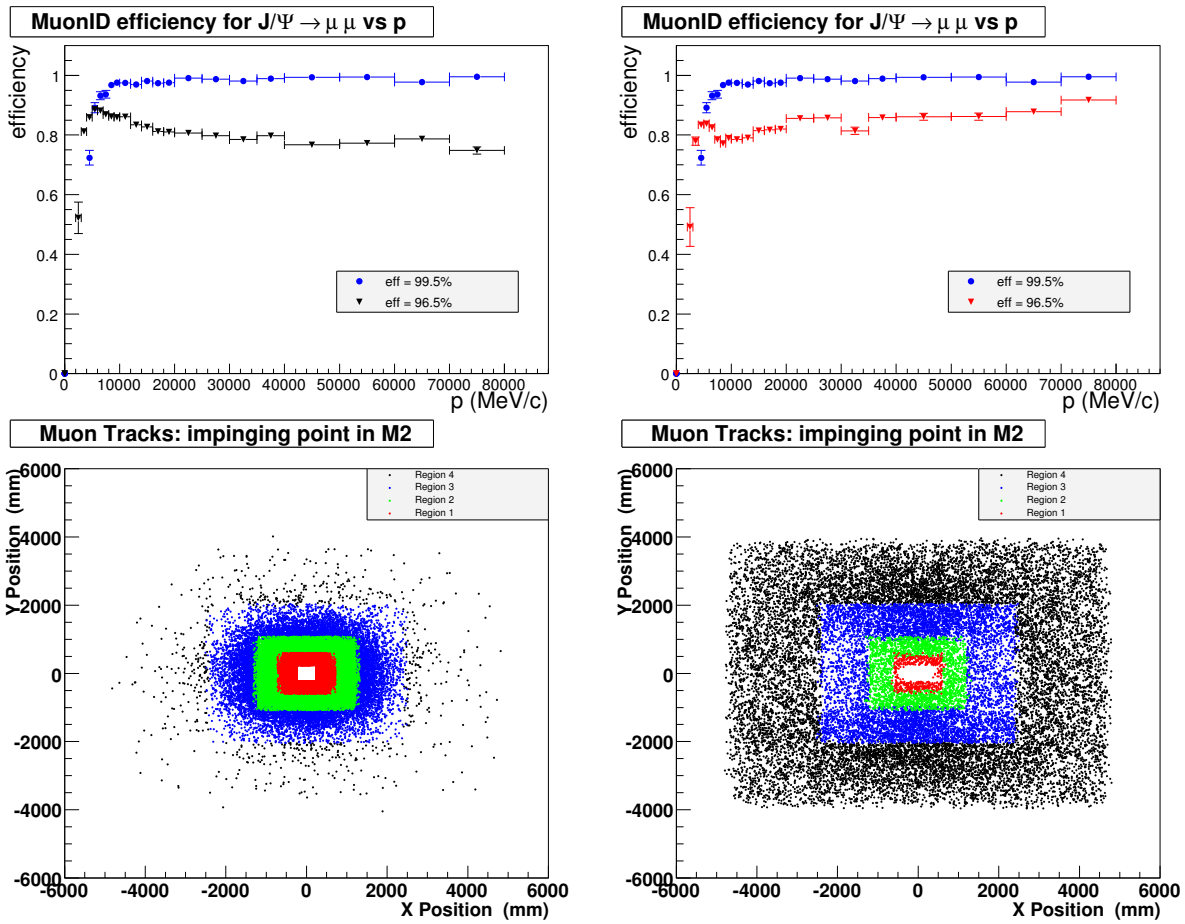

Figure 5: Upper plots: muon identification efficiency for muons coming from an inclusive $J/\Psi \rightarrow \mu\mu$ sample as a function of p. Upper left: blue dots show the MuonID efficiency for MWPC working at nominal efficiency ($\langle\epsilon\rangle = 99.5\%$), black triangles show the effect on the MuonID efficiency of a 3% MWPC efficiency drop in R1 and R2 only. Upper right: blue dots show the MuonID efficiency for MWPC working at nominal efficiency ($\langle\epsilon\rangle = 99.5\%$), red triangles show the effect on the MuonID efficiency of a 3% MWPC efficiency drop in R3 and R4 only. Bottom plots: Muon detector illumination for different momentum ranges, $p > 20$ GeV/c (left) and $3 < p < 10$ GeV/c (right) in different detector regions (R1 in red, R2 in green, R3 in blue and R4 in black).

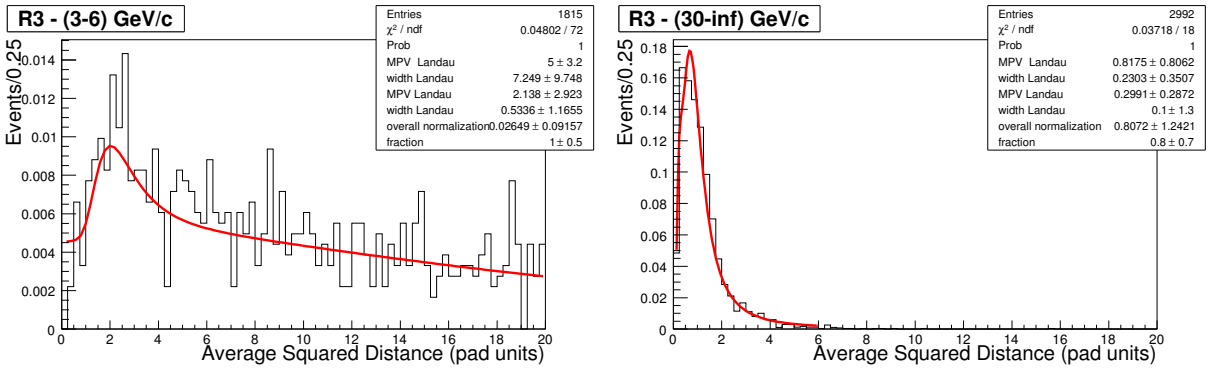

Figure 6: Average squared distance D (see Equation 2) distributions for muons from the $J/\Psi \rightarrow \mu\mu$ decay with momentum $3 < p < 6$ GeV/c (left) and $p > 30$ GeV/c impinging on the R3 region (right).

5.1 The IsMuonLoose definition

In order to have a smoother dependence on the MWPC efficiency a modification of the IsMuon variable, *IsMuonLoose* is introduced. The requirements on the stations to be used in the boolean IsMuonLoose definition are summarized in Table 4: with respect to the IsMuon condition, only two momentum bins are considered and the AND of the stations is changed in OR.

In order to decrease the misidentification of hadron with low momentum each hit can be weighted with the probability for a muon track to reach a particular station, given by the curves shown in Figure 3. This weight is calculated by using the standard hit-or-miss technique to extract the probability that a hit released by a track of a given momentum p is found in a given station.

The probability for a muon of momentum p to reach the stations M2, M3, M4 and M5 has been computed by fitting the curves shown in Figure 3 with the analytical expression:

$$P_i = \frac{(\alpha(p-\beta))^i}{1+(\alpha(p-\beta))^i} \tag{3}$$

with p expressed in MeV/c, α=(0.0260, 0.0021, 0.0015, 0.0008) $(\mathrm{MeV/c})^{-1}$ and β=(2040, 2387, 3320, 3903.) MeV/c for M2,M3,M4 and M5 respectively.

momentum range	stations
3 GeV/c $< p <$ 6 GeV/c	at least one hit in FOI in at least two stations among M2,M3,M4
$p >$ 6 GeV/c	at least one hit in FOI in at least three stations among M2,M3,M4,M5

Table 4: IsMuonLoose decision as a function of momentum range. Each hit is weighted with the probability to reach a given station (see text).

The MuonID efficiency evaluated on a b-inclusive sample with IsMuon/IsMuonLoose definitions is shown in Figure 7 (left).

For chambers working at the nominal working point with an average efficiency of $\langle\varepsilon\rangle \sim 99.5\%$, as it is in the Monte Carlo, the two requirements are almost equivalent as far as the efficiency for muons is concerned, with a tiny gain in the IsMuonLoose case. The results are summarized in Table 5: for muons in a b-inclusive sample we get $\epsilon(\mathrm{IsMuon}) = (95.6 \pm 0.2)\%$ and $\epsilon(\mathrm{IsMuonLoose}) = (97.2 \pm 0.1)\%$.

The IsMuon/IsMuonLoose performance are instead very different in the presence of an even small efficiency loss of the muon chambers: Figure 8 shows the impact of an average efficiency loss of $\sim 2, 4, 6, 8\%$ per chamber with respect to the nominal value, on the MuonID performance for muons using the IsMuonLoose (left) and IsMuon (right) definitions. The MuonID efficiency for muons based on the IsMuonLoose criterion is almost insensitive up to an extreme MWPC efficiency loss of 4-5 % in the whole detector.

However, since the IsMuonLoose definition is looser than IsMuon definition, we expect

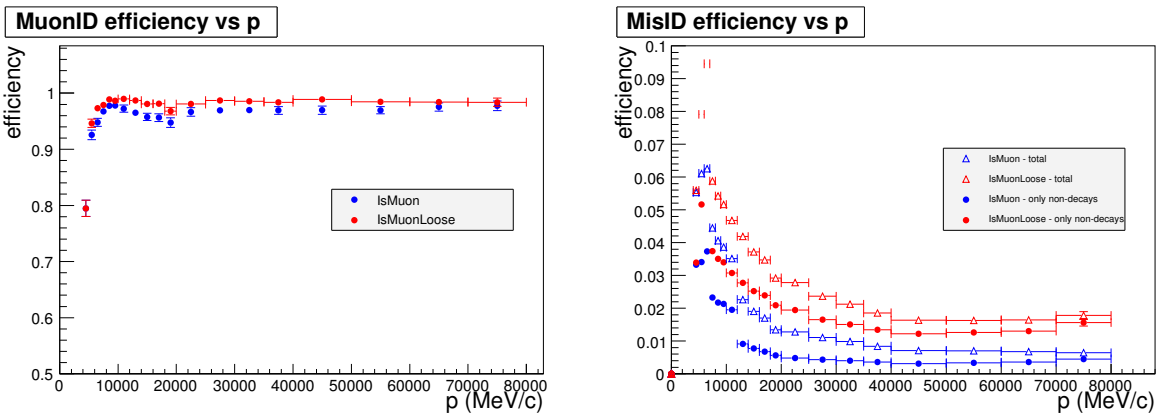

Figure 7: MuonID efficiency (left) and misID rate (right) for the IsMuon/IsMuonLoose definitions. In the misID plots we show separately the contribution the total misID coming from hadrons decaying/non-decaying in flight and the misID only due to non-decays in flight.

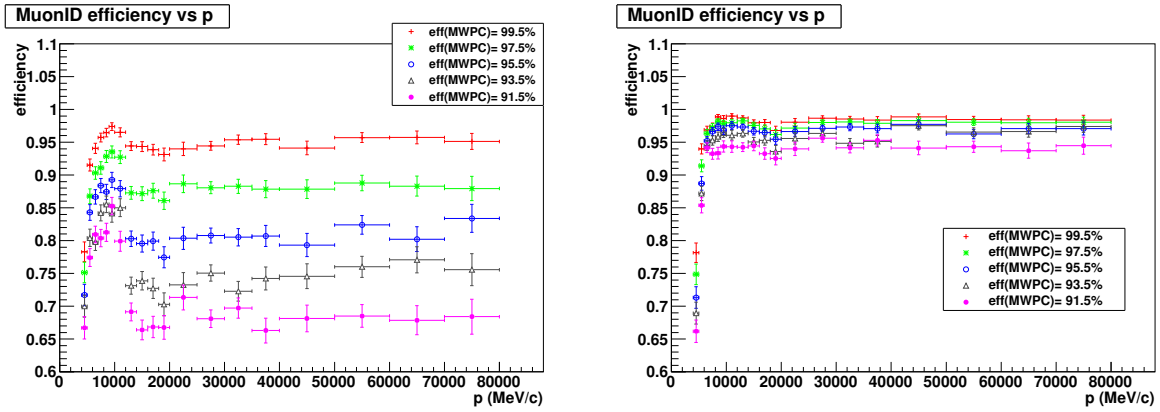

Figure 8: MuonID efficiency for the IsMuon (left) and IsMuonLoose (right) selectors for different average values of the MWPCs efficiency.

an increase of misID rate for the same muon efficiency. The results obtained for a b inclusive sample are shown in Table 5. Here we compare the performance of the IsMuonLoose definition with the IsMuon one in the same momentum bins: we see that the MuonID efficiency is slightly increased (from 96.6% to 97.7%) while the total misID rate increases from 4.3% to 6.5%. The biggest contribution to the increase of misID comes from hadrons, non decaying in flight, with $p > 10$ GeV/c: it increases from $\sim 2.8\%$ (IsMuon) to $\sim 4.9\%$ (IsMuonLoose).

The misID as a function of momentum is shown in Figure 7 (right) for the IsMuon/IsMuonLoose definitions. Red/blue dots show the total misID for the IsMuonLoose/IsMuon definitions, while red/blue triangles show the misID only due to hadrons non decaying in flight.

The MuonID efficiency and misID rate as a function of momentum is shown in Figure 9

for two different samples of muons (b-inclusive and $J/\Psi \rightarrow \mu^+\mu^-$) and two different samples of non-muons (b-inclusive and $\Lambda \rightarrow p\pi$). We notice that for a given p value the curves are very similar. However small differences are present, mainly due to different event topologies and polar angle distributions. These effects must be taken carefully into account in the evaluation of the performance of the algorithm when we will use the calibration samples.

b-inclusive	$3 < p < 6$ GeV/c	$6 < p < 10$ GeV/c	$p > 10$ GeV/c	$p > 3$ GeV/c
MuonID efficiency				
IsMuon	$83.6 \pm 0.9\%$	$95.8 \pm 0.4\%$	$98.3 \pm 0.1\%$	$96.6 \pm 0.2\%$
IsMuonLoose	$85.1 \pm 0.9\%$	$96.9 \pm 0.5\%$	$99.2 \pm 0.1\%$	$97.7 \pm 0.1\%$
IsMuonLoose no weight	$86 \pm 1.0\%$	$96.9 \pm 0.6\%$	$99.2 \pm 0.1\%$	$97.7 \pm 0.2\%$
MisID rate (total)				
IsMuon	$6.6 \pm 0.8\%$	$5.5 \pm 0.6\%$	$2.0 \pm 0.1\%$	$4.3 \pm 0.1\%$
IsMuonLoose	$8.7 \pm 0.8\%$	$7.5 \pm 0.7\%$	$4.3 \pm 0.2\%$	$6.5 \pm 0.2\%$
IsMuonLoose no weight	$10.7 \pm 0.9\%$	$7.8 \pm 0.9\%$	$4.4 \pm 0.3\%$	$7.2 \pm 0.3\%$
MisID rate (non-decays)				
IsMuon	$4.5 \pm 0.6\%$	$3.5 \pm 0.5\%$	$1.1 \pm 0.1\%$	$2.8 \pm 0.2\%$
IsMuonLoose	$6.6 \pm 0.8\%$	$5.6 \pm 0.6\%$	$3.3 \pm 0.2\%$	$4.9 \pm 0.2\%$
IsMuonLoose no weight	$8.6 \pm 0.8\%$	$5.8 \pm 0.8\%$	$3.3 \pm 0.2\%$	$5.6 \pm 0.3\%$

Table 5: MuonID efficiency and MisID rate of the IsMuon vs IsMuonLoose variables for a b-inclusive sample.

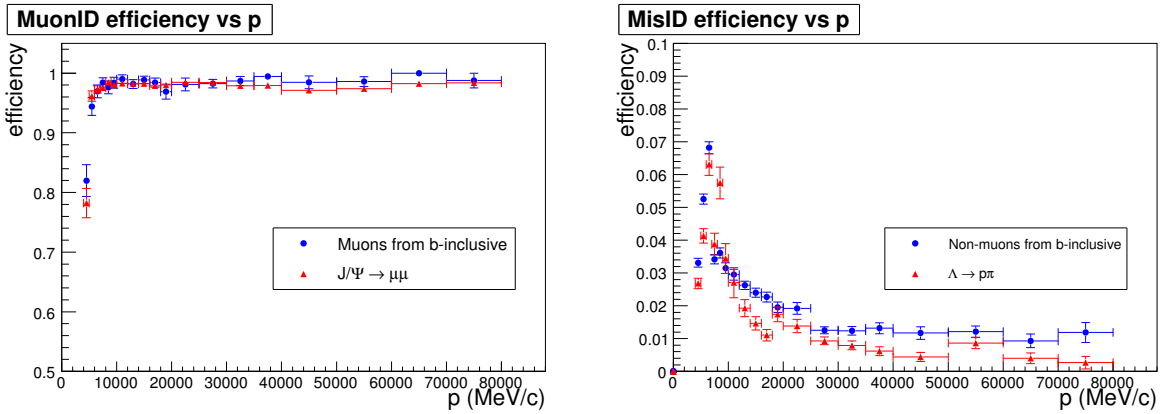

Figure 9: MuonID efficiency versus p for b-inclusive and $J/\Psi \rightarrow \mu^+\mu^-$ samples (right) and MisID rate versus p for b-inclusive and $\Lambda \rightarrow \pi p$ samples (left).

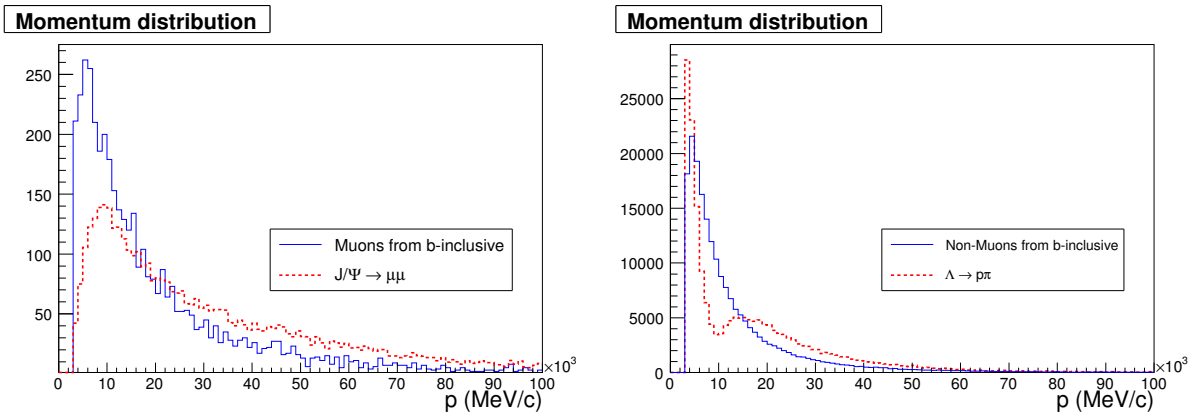

Figure 10: Momentum spectrum for muons from b-inclusive and $J/\Psi \to \mu^+\mu^-$ samples (right) and for hadrons non-decaying in flight from b-inclusive and $\Lambda \to \pi p$ samples (left).

5.2 The binned Delta Log Likelihood

5.2.1 The squared distance variable

The main quantity used to build the Delta Log Likelihood (DLL) is the average squared distance defined in Equation 4. With respect to the definition of distance in Equation 2 only the closest hit to the track extrapolation is considered, as has been found to have a larger discriminant power among muons and non-muons. The new average square distance definition is the following:

$$D = \frac{1}{N}\sum_{i=0}^{N}\left\{\left(\frac{x_{closest,i} - x_{track}}{pad_x}\right)^2 + \left(\frac{y_{closest,i} - y_{track}}{pad_y}\right)^2\right\} \quad (4)$$

where the i runs over the fired stations of the *IsMuonLoose* definition and $x_{closest,i}, y_{closest,i}$ are the coordinates of the closest hit to the track extrapolation for that station.

In Figure 11 we show the D distributions for muons and non-muons from a b-inclusive sample for the definition given in Equation 2 and in Equation 4: we see that the separation between muons and non muons is larger when only the closest hit is considered.

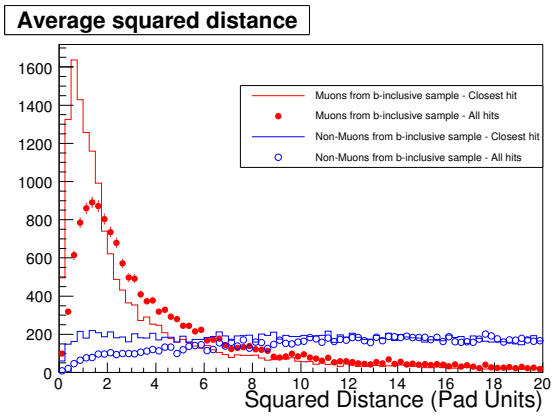

Figure 11: D distributions for muons and non-muons in a b-inclusive sample when we consider only the closest hit (dotted line for muons, solid line for non-muons) or all the hits in FOI (filled circles for muons and open circles for non-muons).

The distribution of the D variable depends on the multiple scattering and, therefore, on the momentum of the track and the amount of material crossed. Since the material crossed by a given track depends on the polar angle of the track itself, D is expected to have a dependence on the polar angle.

In the muon detector each station is subdivided in 4 regions with different readout types and granularity [4]. Therefore it is convenient to parametrize the dependence on the polar angle in terms of the position of the extrapolated track in a given region. For a given region, we evaluate the distribution of the D variable in momentum bins.

The choice of the bin number and size is driven by the time necessary to calibrate the distributions using the two calibration samples $J/\Psi \to \mu\mu$ and $\Lambda \to p\pi$. The number of the bins is the result of a compromise among the accuracy required to calibrate the distribution and the time necessary to collect a reasonable amount of calibration events. The bin size is chosen in order to have almost equally populated bins. A detailed discussion about the use of calibration samples is reported in [1].

In Table 6 we show how the binning is defined: for muons for each region 5 different p-bins are chosen, depending on the region illumination. For region R1 only, two bins more are foreseen at high momentum. For hadrons, where the D dependence with p is weaker, we just divide in regions.

Region	bin 1 p [GeV/c]	bin 2 p[GeV/c]	bin 3 p [GeV/c]	bin 4 p [GeV/c]	bin 5 p [GeV/c]	bin 6 p [GeV/c]	bin 7 p [GeV/c]
R1	$3-10$	$10-20$	$20-30$	$30-40$	$40-50$	$50-60$	$p>60$
R2	$3-10$	$10-20$	$20-30$	$30-40$	$p>40$	–	–
R3	$3-6$	$6-10$	$10-20$	$20-30$	$p>30$	–	–
R4	$3-6$	$6-8$	$8-10$	$10-15$	$p>15$	–	–

Table 6: Definitions of momentum bins for a muon sample.

The average squared distance distributions are evaluated using muons from the $J/\Psi \to \mu\mu$ calibration sample selected as in [1]. They are evaluated for the four muon detector regions and for the momentum bins defined in Table 6 and are shown in Figures 12-13. These distributions are fitted with a double Landau function leaving free all the parameters of the Landau's and the fraction of the second Landau with respect the first one.

The distributions of the D variable for non-muons is obtained from the protons of the $\Lambda \to \pi p$ calibration sample selected as in [1]. They are shown in Figure 14 for the four muon detector regions.

We use only the protons and not the pions of the decay $\Lambda(1115.7) \to \pi p$ as the decay in flight of the pions can fake the distributions: the decays in flight are in fact real muons for the muon system if the decay occurs before M1 and must be treated separately. In the non-muon case the D distribution is fitted with a single Landau.

The D distributions in p, R bins will be calibrated using the two control samples and then exported to signal samples almost without corrections.

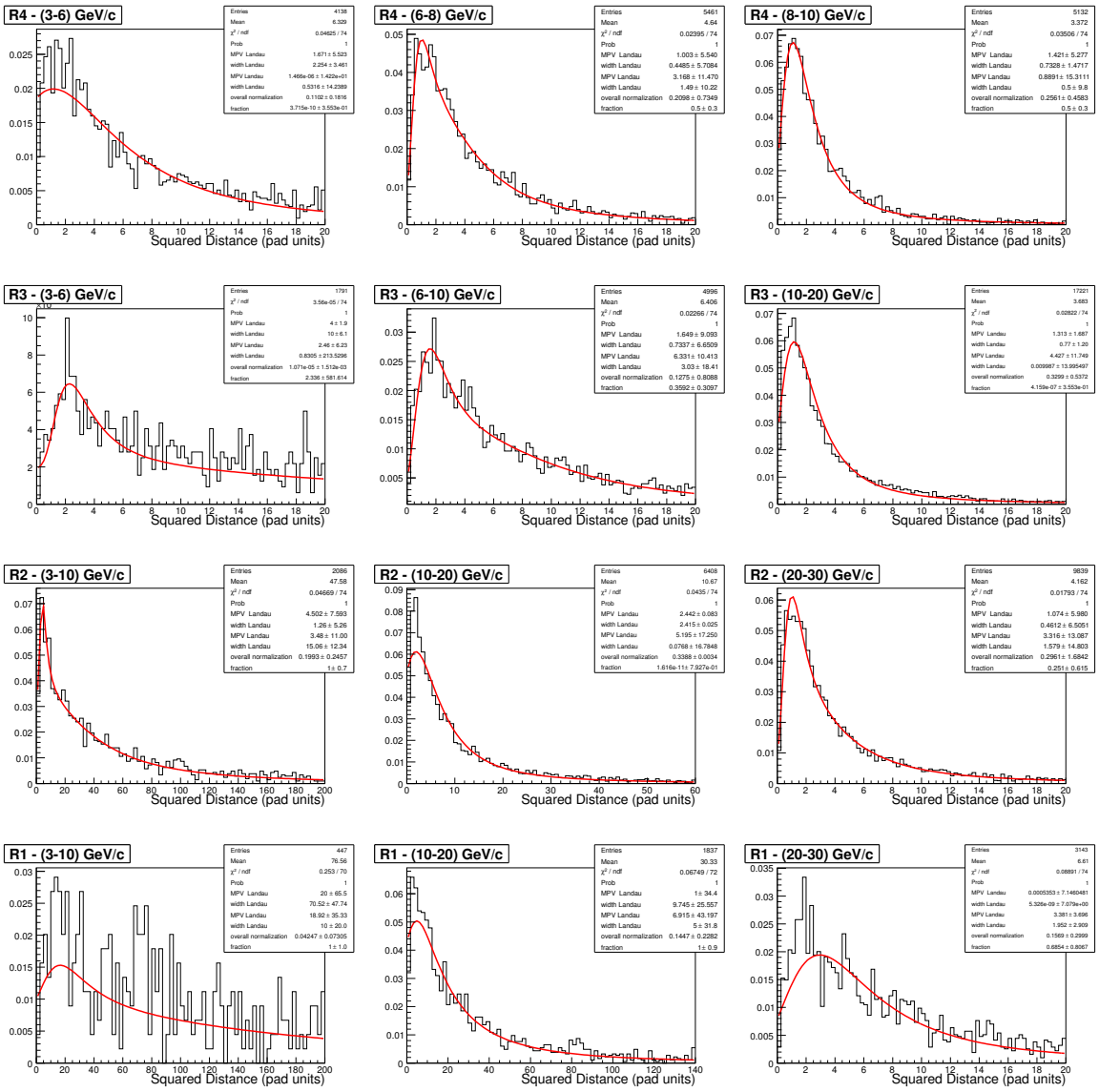

Figure 12: Average square distance distribution for muons from $J/\Psi \to \mu\mu$ inclusive sample for the four Muon Detector regions and for the first three momentum bins as in Table 6.

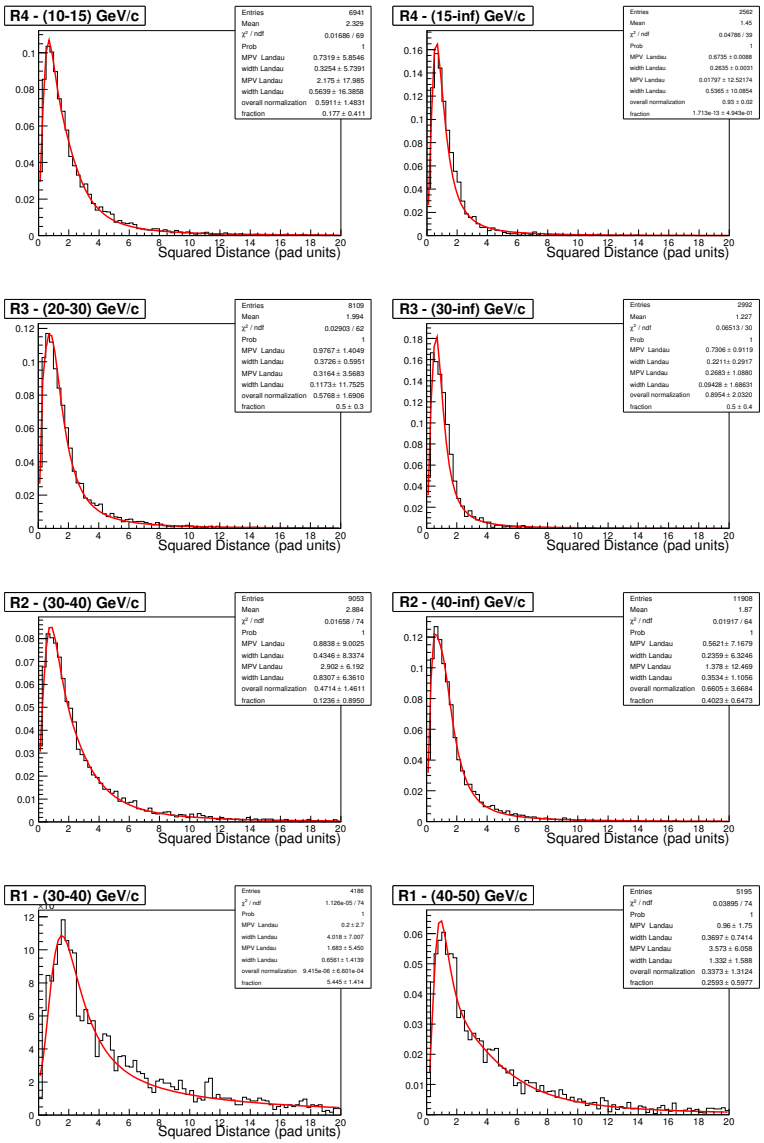

Figure 13: Average squared distance distribution for muons for the 4 Muon Detector regions and for bin 4 and bin 5 as in Table 6.

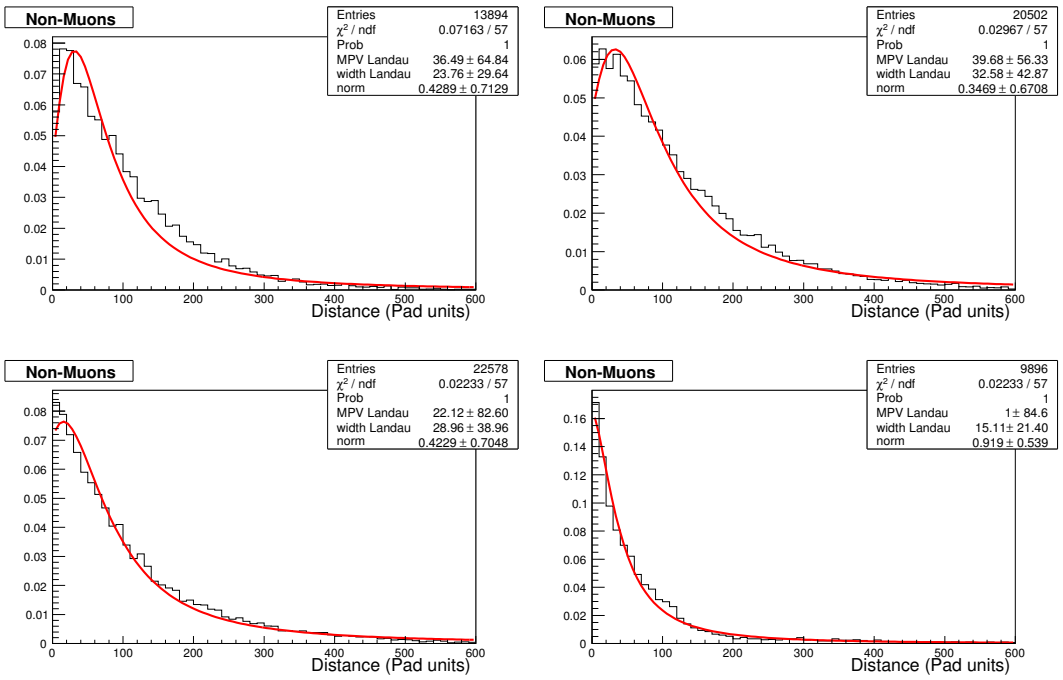

Figure 14: Average squared distance distribution for hadrons non-decaying in flight for the four Muon Detector regions.

5.2.2 The hypothesis test

Given the distributions of the D variable discussed in the previous Section we can make an hypothesis test by giving the probability that a given track of a given momentum p and impinging in a given muon detector region R is a muon or a non-muon.

In general, given a variable D which distributes with a probability distribution function (pdf), if we measure a certain value $D = D_0$, the quantity:

$$P(D_0) = \int_0^{D_0} pdf(D)dD \tag{5}$$

gives the probability that a random experiment will give us $D < D_0$. The cumulative distribution $P(D_0)$, in case of correct and properly normalized pdf, is a uniform distribution between 0 and 1.

In our case we have different pdf for muons and for non-muons depending on the track momentum p and the fired muon detector region R:

$$pdf(D) = pdf_{\mu,\text{non}-\mu}(p, R)$$

as shown in Figures 12-13-14.
If the pdf are correctly normalized, the integral:

$$P_{\mu,h}(D_0) = \int_0^{D_0} pdf_{\mu,h}(p, R, D)dD \tag{6}$$

gives directly the probability that a track with a given (p,R,D_0) is a muon or a non-muon (Figure 15).

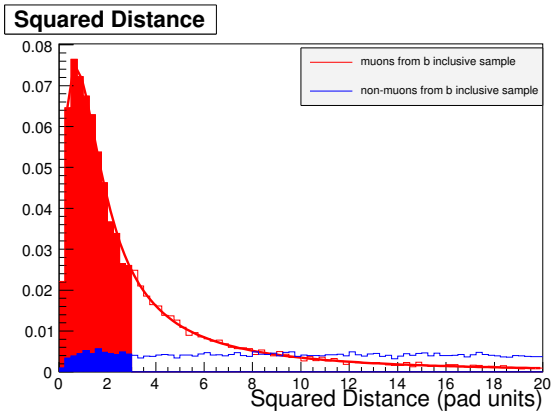

Figure 15: Hypothesis test: definition of the P_μ and $P_{non-\mu}$ probabilities.

Moreover if the parametrization of the curves is correct, in the case of the correct hypothesis the probability has a flat distribution and does not depend on the momentum.

In Figures 17-18 we show the P_μ and $P_{non-\mu}$ distributions for two muons samples (from a b-inclusive sample and from the $J/\Psi \to \mu^+\mu^-$ decay) and for two non-muons samples

(hadrons non-decaying in flight from a b-inclusive sample and from $\Lambda \rightarrow p\pi$ sample) integrated over all the momentum spectrum and detector regions.

We see that in the case of correct hypothesis the distributions are flat as expected. This is shown also in Figure 16 where the P_μ for muons from a b-inclusive sample is shown as a function of p: there is no dependence with the momentum. The residual non-flat behavior is an intrinsic limit due to the finite number of bins in p and in p_t (or Region) we subdivided the sample.

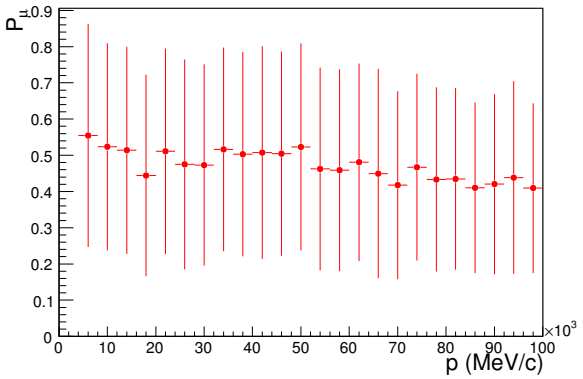

Figure 16: Average probability $< P_\mu >$ for muons from a b-inclusive sample as a function of momentum.

In case of wrong hypothesis we have instead two possibilities:

1. assume we want to evaluate the probability to be a muon for a hadron non-decaying in flight: since we measure a D_0 very large with respect to the D expected for a muon, the integral $P_\mu(D_0)$ given by Equation 6 is a number very close to 1 (Figure 17), or $1 - P_\mu(D_0)$ is a number very close to 0;

2. assume we want to evaluate the probability to be an hadron non-decaying in flight for a muon: since we measure a D_0 very small with respect to the D expected for a hadron the integral $P_{\mathrm{non}-\mu}(D_0)$ given by Equation 6 is a number very close to 0 (Figure 18), or $1 - P_{\mathrm{non}-\mu}(D_0)$ is a number very close to 1.

To use $P_{\mu,\mathrm{non}-\mu}$ or $1 - P_{\mu,\mathrm{non}-\mu}$ is just a matter of convention. We choose to use $P_{\mu,\mathrm{non}-\mu}$ since in this case, for the muon hypothesis, the integral is less affected by the parameterizations of the tails, which are less precisely determined with respect to the core of the distributions.

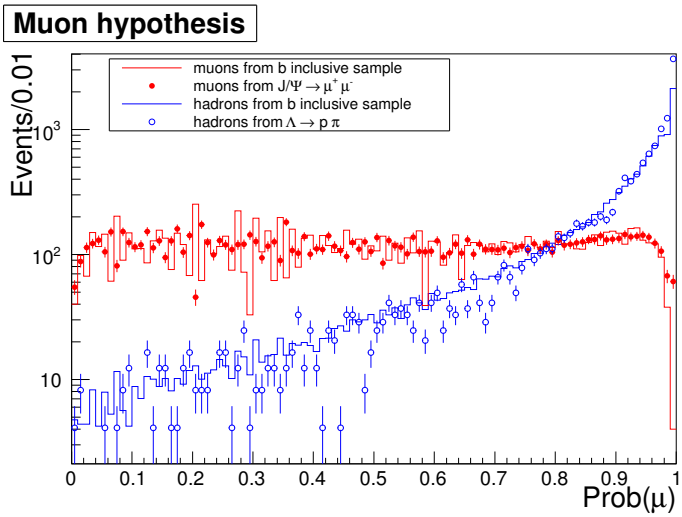

Figure 17: Probability to be a muon for muons and hadrons (non-decaying in flight) samples.

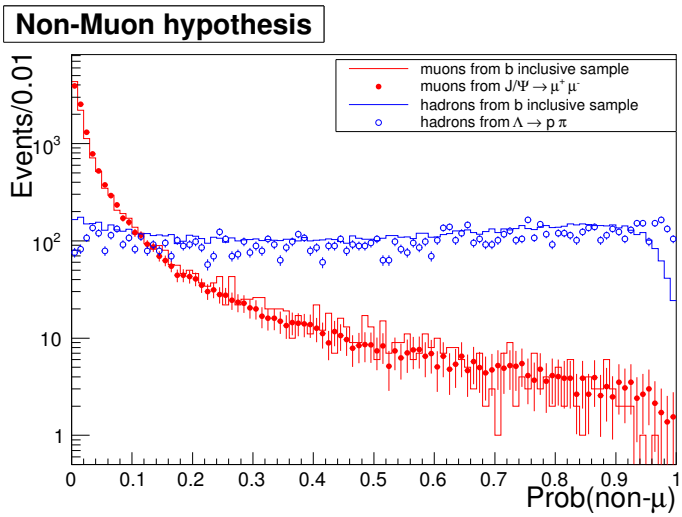

Figure 18: Probability to be a non-muon for muons and hadrons (non-decaying in flight) samples.

6 Results

Once we have for a given track the probability to be a muon (P_μ) or a non-muon ($P_{non-\mu}$) we can build a Delta Log Likelihood defined as:

$$DLL = log(P_\mu / P_{non-\mu}).$$

The distribution of the DLL for muons and non-muons samples is shown in Figure 19. The distributions obtained from a b-inclusive sample are overlaid with the ones obtained from the calibration samples $J/\Psi \rightarrow \mu\mu$ and $\Lambda \rightarrow p\pi$.

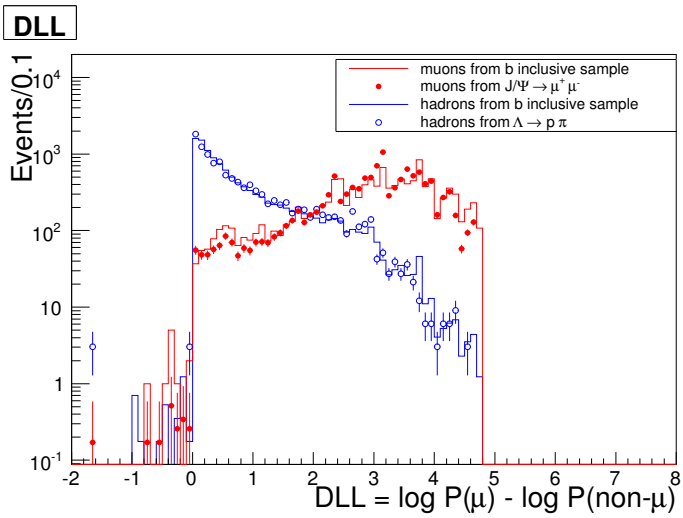

Figure 19: Delta Log Likelihood for muons and non-muons samples.

We have seen in the previous Section that, in case of correct hypothesis, P_μ and $P_{non-\mu}$ do not depend on the momentum. However, in case of wrong hypothesis, P_μ and $P_{non-\mu}$ depend on the momentum of the track: in fact a muon is much more *non-muon like* if it has low momentum, since the large multiple scattering produces larger values for D. This is shown in Figure 20 (left) where the $P_{non-\mu}$ for a muon sample is shown as a function of p.

Since the DLL is defined as the ratio between correct and wrong hypothesis we expect a dependence with p due to the wrong hypothesis part: this is actually observed by plotting the DLL versus the momentum (Figure 20, right).

In Figure 21 we show the MuonID efficiency versus the misidentification rate for different cuts on the P_μ and DLL: we see that the $DLL = log(P_\mu / P_{non-\mu})$ has a bigger discriminant power between muons and non-muons with respect to the simpler P_μ hypothesis. On the other hand, a cut in DLL modifies the original spectrum of the muons as it cuts aways more low-momentum particles while P_μ, by construction, is uniform on the whole spectrum.

This is shown in Figure 22 where we show the muonID efficiency as a function of p for different DLL cuts (left) and P_μ cuts (right): we see that a cut on DLL produces a drop in efficiency mainly in the low-momentum range, while a cut on P_μ removes almost uniformly all the events in the whole range.

Finally in Tables 7- 8 we show the results for a generic b-inclusive sample. We show separately the efficiency for muons (ϵ_μ, the total efficiency on non-μ tracks ($\epsilon_{\text{non}-\mu}$ total), the efficiency for non-muon tracks excluding hadrons which decay in flight ($\epsilon_{\text{non}-\mu}$, non-decays in flight) and efficiency on π's and K's decays in flight ($\epsilon_{\text{non}-\mu}$, decays in flight) after the IsMuonLoose request and after different cuts on the DLL (Table 7) and on P_μ (Table 8).

The use of the DLL or the P_μ distributions to reduce the background contamination depends on the analysis: for analyses that care about the kinematics of the final muon sample it is recommended the use of P_μ as we have seen, this variable does not introduce any bias in the momentum spectrum. For analyses that, instead, do not care about the kinematics of the final sample it is recommended the use of DLL as this ensures a larger discriminant power between muons and non-muons (Tables 7- 8).

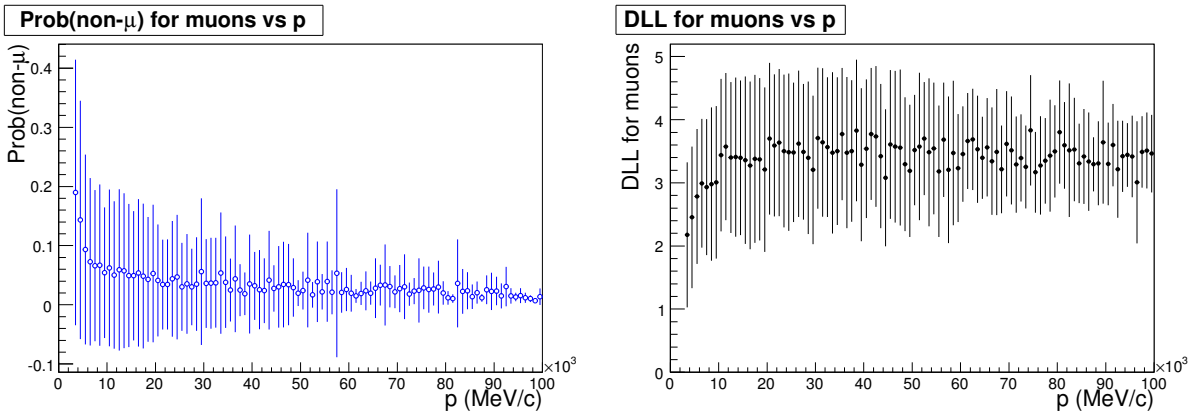

Figure 20: Momentum dependence of the $P_{non-\mu}$ for a muon sample.

DLL cut	ϵ_μ [%]	$\epsilon_{\text{non}-\mu}$ [%] (total)	$\epsilon_{\text{non}-\mu}$[%] (non decays in flight)	$\epsilon_{\text{non}-\mu}$[%] (decays in flight)
>0.0	98.6 ± 0.5	7.3 ± 0.07	5.20 ± 0.06	72.6 ± 0.9
>0.4	97.4 ± 0.5	5.26 ± 0.07	3.18 ± 0.06	66.7 ± 0.9
>0.6	96.4 ± 0.6	4.47 ± 0.07	2.63 ± 0.06	63.0 ± 1.0
>0.8	95.2 ± 0.7	3.80 ± 0.07	2.06 ± 0.05	59.0 ± 1.0
>1.0	94.2 ± 0.8	3.30 ± 0.06	1.66 ± 0.05	55.0 ± 1.0
>1.2	92.1 ± 0.9	2.86 ± 0.06	1.32 ± 0.04	51.0 ± 1.0
>1.4	89.8 ± 0.9	2.46 ± 0.06	1.03 ± 0.04	47.0 ± 1.0

Table 7: Efficiency for muons, total efficiency for non-muon tracks, efficiency for non-muon tracks excluding the decays in flight and efficiency for π's and K's decays in flight from a b-inclusive sample as a function of the DLL cut.

$Prob_\mu$ cut	ϵ_μ[%]	$\epsilon_{\text{non}\mu}$[%] (total)	$\epsilon_{\text{non}\mu}$[%] (non decays)	ϵ_{decays} [%] (decays)
<0.95	93.9 ± 0.4	4.58 ± 0.04	2.83 ± 0.03	58.2 ± 0.5
<0.90	89.1 ± 0.5	3.41 ± 0.03	1.94 ± 0.03	49.8 ± 0.5
<0.85	83.6 ± 0.6	2.71 ± 0.03	1.41 ± 0.02	43.6 ± 0.5
<0.80	79.3 ± 0.7	2.24 ± 0.03	1.06 ± 0.02	39.2 ± 0.5
<0.75	74.7 ± 0.7	1.88 ± 0.02	0.82 ± 0.02	35.4 ± 0.5
<0.70	70.1 ± 0.7	1.61 ± 0.02	0.63 ± 0.01	32.2 ± 0.5

Table 8: Efficiency for muons, total efficiency for non-muon tracks, efficiency for non-muon tracks excluding the decays in flight and efficiency for π's and K's decays in flight from a b-inclusive sample as a function of the P_μ cut.

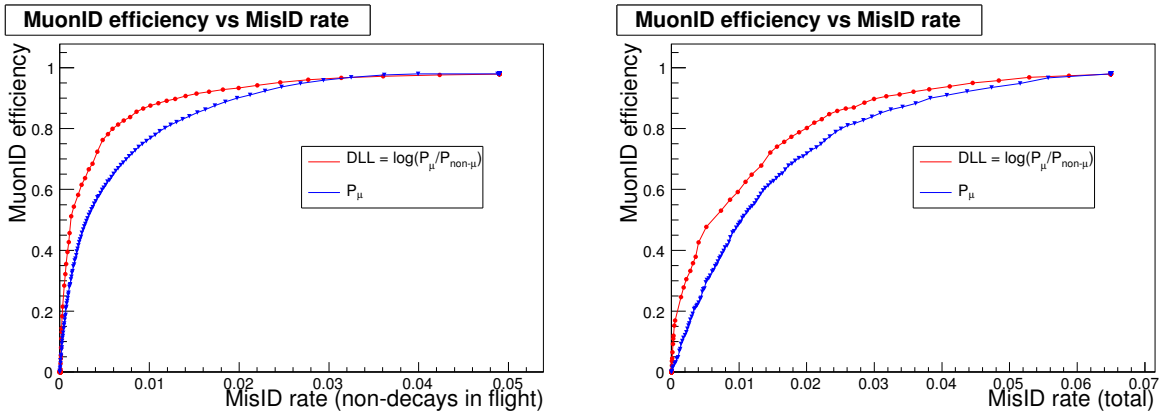

Figure 21: MuonID efficiency versus misID rate for a b-inclusive sample, for different DLL cuts (red filled circles) and P_μ cuts (blue open circles). Left: misID rate for hadrons non-decaying in flight. Right: total misID rate.

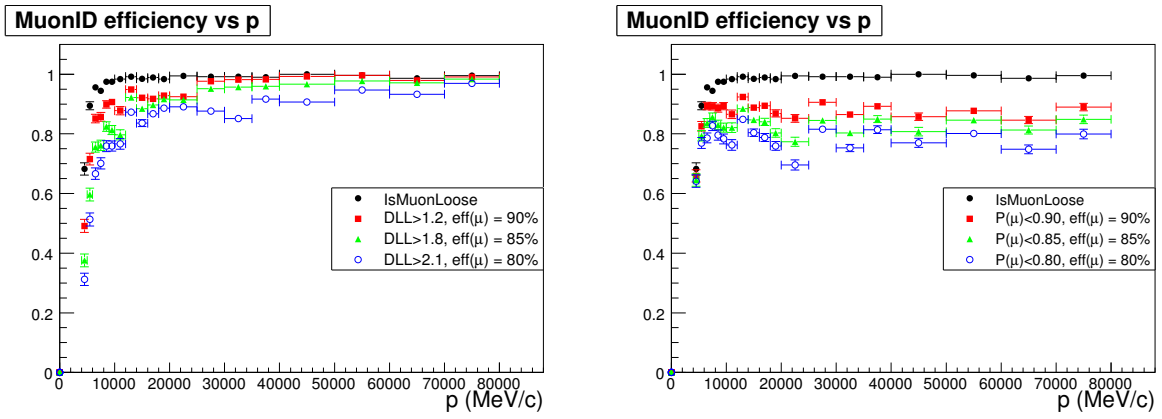

Figure 22: MuonID efficiency for b-inclusive sample, for different cuts on $DLL = log(P_\mu/P_{non-\mu})$ (Left) and on P_μ (Right).

7 MuonID with the Calorimeters with first data

The Calorimeter System of LHCb [10] comprises a SPD, Pre-shower Detector, an Electromagnetic Calorimeter (ECAL) and a Hadronic Calorimeter (HCAL).

The energy deposited in the electromagnetic and hadronic calorimeters can be used as a discriminant variable to increase the discriminating power between muons and non-muons: in fact, since muons are Minimum Ionizing Particles (MIPs), this energy is a fixed quantity which depends only on the dE/dX in the calorimeter material, while for electrons and hadrons it depends on the energy of the particles.

In Figure 23 we show the energy released in ECAL and HCAL by muons and non-muons from a b-inclusive sample after the IsMuonLoose condition. We see that in ECAL a MIP releases on average around $\sim$ 400 MeV while in HCAL $\sim$ 2200 MeV.

In Figure 24 we show the same distributions by dividing the sample in four sub-samples of tracks pointing in the four regions of the Muon System: the peaks at zero visible mainly in the ECAL distributions are due to the fact that below a certain polar angle the MIP signal goes below threshold and is not detected [11].

The energy released along the track trajectory can be used to perform a hypothesis test and to assign to a given track the probability to be a muon or a non-muon [12]. These probabilities can be combined with the P_μ and $P_{\mathrm{non}-\mu}$ given by the muon system and by other sub detectors into a *combined* DLL [13].

However, to have the DLL of all the sub detectors properly calibrated and merged together will require some time. Therefore we can envisage in the first period of data taking to improve the rejection power between muons and non-muons by using the calorimeter information in a simpler way, just cutting on the MIPs distributions.

In Figure 25 we show the MuonID efficiency and misID rate for tracks surviving the IsMuonLoose condition as a function of the maximum energy released in ECAL and HCAL. These curves can be used as additional handles to improve the rejection power at the beginning of data taking.

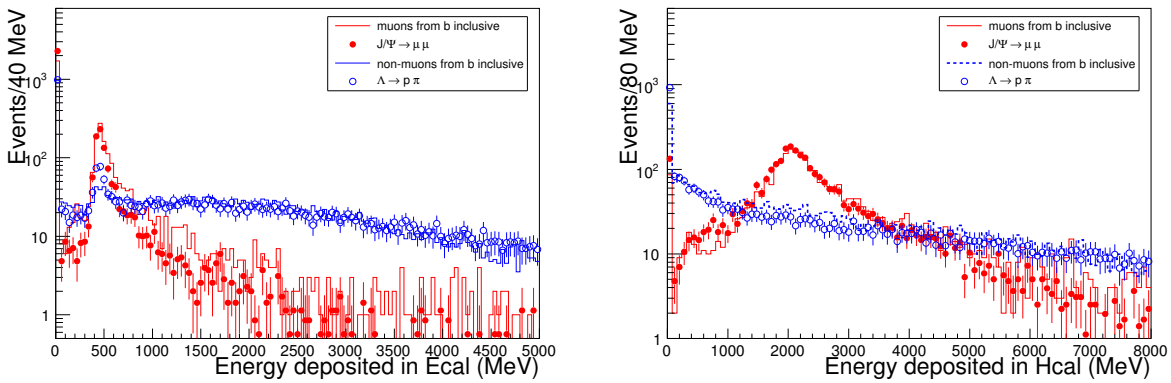

Figure 23: Energy deposited in the Electromagnetic Calorimeter (left) and in the Hadronic calorimeter (right) by muons from a b inclusive sample (solid line), muons from $J/\Psi \rightarrow \mu\mu$ (filled circles), non-muons from a b-inclusive sample (dashed line) and non-muons from $\Lambda \rightarrow p\pi$ (open circles).

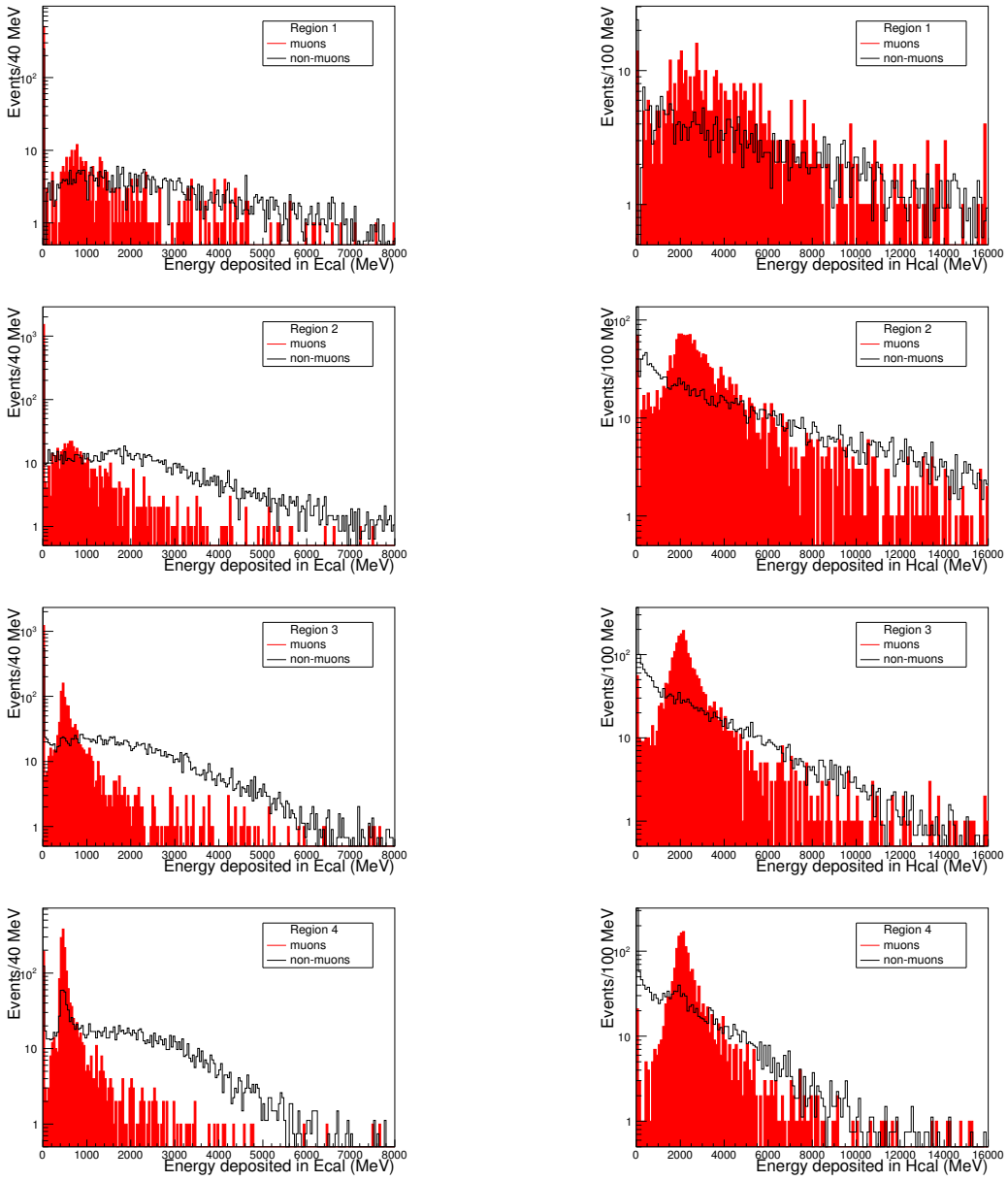

Figure 24: Energy deposited in the Electromagnetic Calorimeter (left) and in the Hadronic calorimeter (right) by muons (filled histograms) and non-muons (solid line) pointing in the four muon detector regions. In the non-muons sample has been removed the contribution of decays in flight.

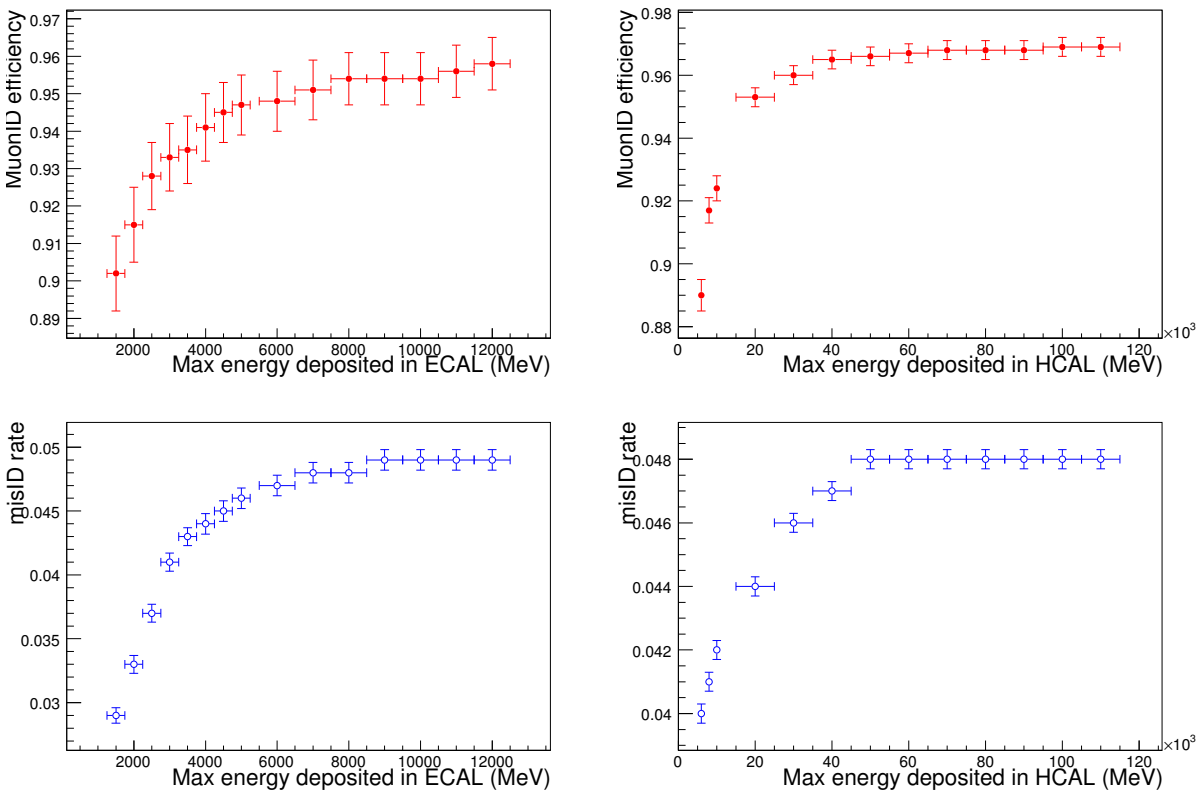

Figure 25: MuonID efficiency (top) and misID rate (bottom) as a function of the maximum energy released in ECAL (left) and HCAL (right).

8 Combined MuonID performance

The MuonID performance can be further improved by combining in a global Likelihood the the informations coming from all the subdetectors, mainly Calorimeters and RICHs [13].

The combined Delta Log Likelihood (combDLL) distributions for muons and non-muons are shown in Figure 26. In the same Figure 26 (right) we show the MuonID efficiency versus misID rate (total and without the contribution of π's and K's decays in flight) as a function of a the combined DLL cut. In Table 9 we show the results obtained by applying a cut on the combined DLL distribution corresponding to a MuonID efficiency of 99%, 98%, 95% and 90%. For comparison, in Table 10 we show the results obtained when we apply a cut on the DLL distribution of the Muon system alone corresponding to the same MuonID efficiency values.

We see that in the high efficiency range ($> 90\%$) the combined likelihood allows to improve by almost $\sim 50\%$ the rejection of the non-muon tracks with respect to the DLL from the muon system alone while keeping the same muon efficiency. This is due to a higher suppression both of π's and K's decays in flight which are efficiently identified by other subdetectors and of spurious hits in the muon chambers that contribute to the misID of hadrons non decaying in flight.

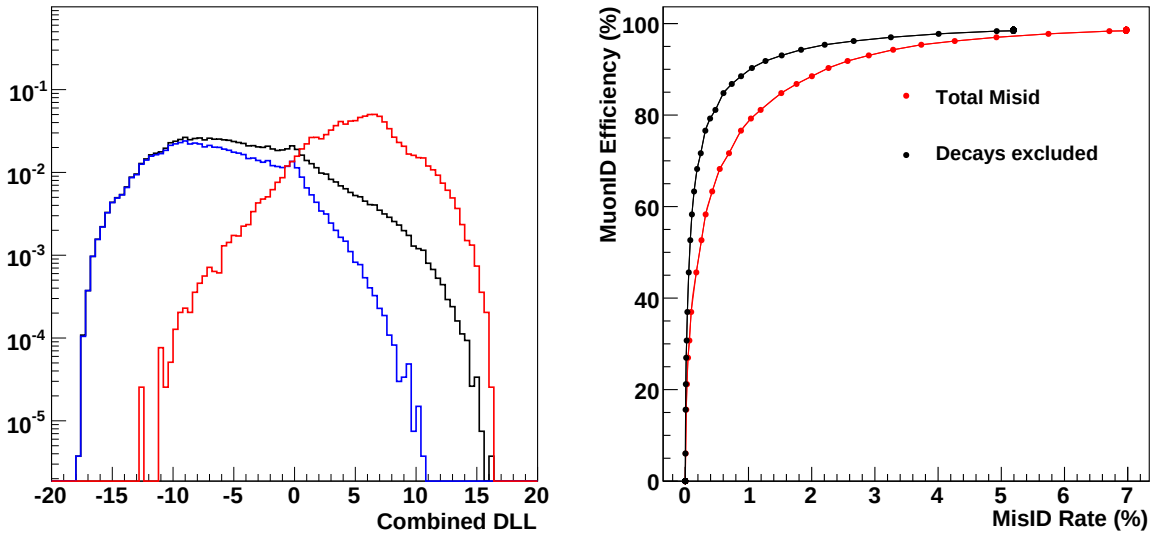

Figure 26: Left: combined DLL distribution for muons (red), non-muons (black) and non-muons after removing the contribution of π's and K's decays in flight (blue) from a b inclusive sample. Right: MuonID efficiency vs misID rate (total: black dots; without the contribution of π's and K's decays in flight: red dots) as a function of the combined DLL cut.

combDLL cut	ϵ_μ [%]	$\epsilon_{\text{non}-\mu}$ [%] (total)	$\epsilon_{\text{non}-\mu}$[%] (non decays in flight)	$\epsilon_{\text{non}-\mu}$[%] (decays in flight)
>-20.0	98.66 ± 0.06	6.98 ± 0.01	5.19 ± 0.01	69.1 ± 0.1
>-5.20	97.97 ± 0.07	3.69 ± 0.01	2.191 ± 0.008	55.8 ± 0.2
>-1.60	94.8 ± 0.1	2.355 ± 0.008	1.230 ± 0.006	41.5 ± 0.2
>0.0	90.7 ± 0.1	1.816 ± 0.007	0.880 ± 0.005	34.3 ± 0.2

Table 9: Combined DLL: efficiency for muons, total efficiency for non-muon tracks, efficiency for non-muon tracks excluding the decays in flight and efficiency for π's and K's decays in flight from a b-inclusive sample as a function of the combined DLL cut.

DLL cut	ϵ_μ [%]	$\epsilon_{\text{non}-\mu}$ [%] (total)	$\epsilon_{\text{non}-\mu}$[%] (non decays in flight)	$\epsilon_{\text{non}-\mu}$[%] (decays in flight)
>0.0	98.6 ± 0.5	7.3 ± 0.07	5.20 ± 0.06	72.6 ± 0.9
>0.4	97.4 ± 0.5	5.26 ± 0.07	3.18 ± 0.06	66.7 ± 0.9
>0.8	95.2 ± 0.7	3.80 ± 0.07	2.06 ± 0.05	59.0 ± 1.0
>1.4	89.8 ± 0.9	2.46 ± 0.06	1.03 ± 0.04	47.0 ± 1.0

Table 10: Muon DLL: efficiency for muons, total efficiency for non-muon tracks, efficiency for non-muon tracks excluding the decays in flight and efficiency for π's and K's decays in flight from a b-inclusive sample as a function of the combined DLL cut.

The combined procedure will be probably not used in the first period of data taking as it requires the calibration of each subdetector and a full understanding of the performance of all the particle identification algorithms involved. However it allows to reach better performance and it is therefore recommended as soon as all the particle identification procedures are well established.

9 Conclusions

An improved MuonID procedure for the LHCb experiment has been presented. This procedure is robust against possible Muon Detector inefficiencies so it is well suited for first data taking when the detector behavior could be still not optimal. Moreover the new algorithm takes properly into account the momentum dependence so it can be calibrated with control samples and exported to signal samples with different momentum spectra without large corrections.

The hypothesis test has been performed both using the simple "muon-hypothesis" and the ratio between *muon* and *non-muon* hypotheses: the first case does not modify the momentum spectrum of the muon sample and therefore is more suitable for analyses which care about the kinematics of the event. The second case modifies the momentum spectrum but has a larger discriminant power, so it is more convenient for analyses which require a high rejection of the backgrounds.

The average performance depends on the momentum spectrum of the analyzed sample: with the present simulation for a generic b-inclusive sample we find a muon identification efficiency of 90% for a misidentification rate of $\sim$2.4% ($\sim$ 1% excluding π's and K's decays in flight) for tracks with $p > 3$ GeV/c.

Additional rejection power can be obtained by combining in a proper way the informations coming from all the other subdetectors in a global Likelihood: for the same sample we find a muon identification efficiency of 90% for a misidentification rate of $\sim$1.8% ($\sim$ 0.8% excluding π's and K's decays in flight).

10 Acknowledgements

We want warmly to thank the whole *Trigger and Reconstruction* Working Group for lively discussions and fruitful collaboration, in particular T. Ruf and C. Jones for their precious help in finalizing this work and editing the note.

References

[1] S. Furcas, G. Lanfranchi, A. Sarti, M. Palutan, *Calibration strategy and Efficiency Measurement of the Muon Identification Procedure at LHCb*, LHCb note 2009-0xx, (2009).

[2] X. Cid Vidal, J. A. Hernando Morata, *The use of the Kalman fit for the MuonID procedure of the LHCb experiment* LHCb 2009-yyy (2009).

[3] E. Polycarpo, M. Gandelman, *The Performance of the LHCb Muon Identification Procedure*, LHCb note 2007-145 (2007).

[4] LHCb Collaboration, *LHCb Muon System TDR*, CERN/LHCC 2001-010 (2001), *Addendum to the Muon System TDR*, CERN/LHCC 2003-002 (2003) and *Second Addendum to the Muon System TDR*, CERN/LHCC 2005-012 (2005).

[5] M. Anelli et al., *Extensive aging test of two prototypes of four-gap MWPC for the LHCb Muon System*, CERN-LHCb 2004-029.

[6] M. Anelli et al., *Test of MWPC Prototypes for Region 3 of Station 3 of the LHCb Muon System*, CERN-LHCb 2004-074.

[7] M. Anelli et al., *Test of a four-gap MWPC for the LHCb Muon System at the Gamma Irradiation Facility at CERN*, CERN-LHCb 2005-003.

[8] The LHCb Collaboration, *The LHCb Technical Proposal*, CERN/LHCC 98-004.

[9] BRUNEL, the LHCb event reconstruction program, http://lhcb-release-area.web.cern.ch/LHCb-release-area/DOC/brunel/.

[10] *LHCb Calorimeters, Technical Design Report*, CERN-LHCC-2000-049.

[11] I. Korolko et al., *On the possibility of in situ calibration of LHCb calorimeters*, CERN-LHCb-2000-051.

[12] H. Terrier and I. Belyaev, *Particle identification with LHCb calorimeters* CERN-LHCb-2003-092.

[13] https://twiki.cern.ch/twiki/bin/view/LHCb/GlobalParticleID.